Optical microrotors: theory, design and fabrication

Vincent L. Y. Loke, Theodore Asavei, Timo A. Nieminen,
Norman R. Heckenberg and Halina Rubinsztein-Dunlop

Centre for Biophotonics and Laser Science, School of Physical Sciences,
The University of Queensland, Brisbane QLD 4072, Australia

ABSTRACT

Building on the ability to exert torques in optical tweezers, optically-driven rotating micromachines have reached the verge of practical application. Prototype devices have been made, and useful applications are being sought. We outline some general principles that can be applied to the design of optically-rotated devices, and describe a method for rigorous computational modelling that is well-suited to the optimization and engineering of such micromachines. Finally, we describe a method for rapid microfabrication of prototypes for testing, and some results of such tests.

Keywords: Optical tweezers, micromanipulation, micromachines, MEMS, optical torque

1. INTRODUCTION

Optically-driven micromachines are an interesting and possibly practically useful outgrowth of optics tweezers. A significant amount of work has already been carried out, which we recently reviewed,[1] prototype devices are being constructed,[2,3] and potential real-world applications for the technology are being sought. Thus, it is timely to present the processes that we employ for the design and fabrication of optically-driven microdevices.

We first briefly review the theory of optical torques, and discuss the implications of the theory for qualitative principles of design. Next, we consider the quantitative modelling of such devices, and discuss one highly suitable method in detail. Finally, we describe our procedure for rapid microfabrication of prototype devices.

2. THEORY

That light can carry angular momentum is a direct consequence of the transport of linear momentum, which in turn, follows from the transport of energy by light. Accordingly, the energy flux or beam power P is perhaps the most important parameter. If we have a monochromatic paraxial Gaussian beam of power P, then the momentum flux[4,5] is

$$\vec{p} = nP/c \tag{1}$$

in the direction of propagation of the beam, where n is the refractive index of the medium, and c is the speed of light in free space. For the most common case of plane polarization, the angular momentum flux is zero. However, for the arguably more basic case of circular polarization, the angular momentum flux is

$$\vec{J} = P/\omega, \tag{2}$$

either parallel or anti-parallel to the direction of beam propagation, where ω is the optical angular frequency.

The scaling of optical angular momentum with frequency has an interesting consequence. It would appear that more and more torque should be available for a given beam power if the frequency is reduced (c.f. the use of low frequency power supplies—25 Hz or lower—for greater efficiency in applications such as electric locomotives, which also fundamentally depend on the electromagnetic transport of angular momentum). However, the diffraction-limited focal spot size also increases in inverse proportion to the frequency if the frequency is reduced, and if the focal spot becomes larger than the object being optically-driven, the non-intercepted portion of the beam is wasted. Therefore, for a given target object, the most efficient optical drive using a circularly polarized beam results when

- the beam is focused to a diffraction-limited spot, and

Optical Trapping and Optical Micromanipulation IV, edited by Kishan Dholakia, Gabriel C. Spalding,
Proc. of SPIE Vol. 6644, 66440U, (2007) · 0277-786X/07/$18 · doi: 10.1117/12.735341

- the frequency is such that the overlap between the diffraction-limited spot and the target is maxmized.[6,7]

The former of these suggests a close alliance between optically-driven micromachines and conventional optical tweezers. The latter is clearly impractical, given the need for optical components suitable for each wavelength in use. However, while the angular momentum carried through circular polarization is restricted to $\pm\hbar$ per photon since it is *spin* angular momentum and subject to this maximum for electromagnetic fields, angular momentum can also consist of *orbital* angular momentum as well, which is subject to no such limit. In general, we can have a paraxial beam such that

$$\vec{J} = (\sigma_z + \ell)P/\omega, \tag{3}$$

where σ_z is the degree of circular polarization and ℓ is the orbital angular momentum per photon about the beam axis. Notably, the Laguerre–Gauss modes[8] are eigenfunctions of the angular momentum, and each mode is characterized by an integer value of orbital angular momentum per photon.[9,10]

The diffraction-limited focal spot of a Laguerre–Gauss mode is proportional to the angular momentum,[11] so, by employing orbital angular momentum instead of a change in frequency, efficient optical drive results when

- the beam is focused to a diffraction-limited spot, and
- the orbital angular momentum per photon, ℓ, is such that the overlap between the diffraction-limited spot and the target is maxmized.[6,7]

Clearly, larger micromachines require the use of orbital angular momentum efficiency.

2.1. Transfer of Angular Momentum

The transfer of angular momentum from the driving beam to the target object is essentially a scattering process. If the angular momentum flux of the scattered field differs from that of the driving field, then there is a non-zero optical torque. The most important influence on the details of the scattering process is the rotational symmetry of the scattering object. We have discussed this in detail elsewhere,[7] and will only give a brief outline here.

Firstly, if the object is rotationally symmetric, the angular momentum per photon, as measured about the axis of symmetry, cannot be changed.[12,13] A torque can only result from a change in photon flux, by absorption (or, in principle, by gain). However, the resulting heating makes this an impractical method.

Therefore, there must be some deviation from rotational symmetry. This can either be microscopic, whereby the electromagnetic properties, such as the permittivity tensor, break this symmetry, or macroscopic, where the shape of the particle breaks the rotational symmetry. The simplest cases are the use of birefringent particles[14] or elongated particles.[15] The idea of form birefringence[16] unites these two. However, birefringence is best suited to small particles; by their nature, such particles are driven by spin angular momentum, and are therefore optimum when comparable in size to a diffraction-limited Gaussian beam.

In seeking shapes that can be optimally driven by high orbital angular momentum beams, we need to consider the coupling between the incident and scattered light. Essentially, if an object has discrete rotational symmetry—typical of almost all optically-driven micromachines so far—the difference between angular momenta of incident and scattered modes will be equal to an integer times the order of discrete rotational symmetry.[7] In addition, the most effective scattering processes producing torque are usually first-order scattering, wherein the angular momentum difference is equal to the order of symmetry, and scattering to the lowest angular momenta available. This suggests that if we drive micromachines using incident orbital angular momentum, the order of discrete rotational symmetry should be approximately equal to the incident angular momentum per photon.

Similarly, a device intended to be driven by an incident Gaussian beam should have an order of symmetry such that the scattered light will carry the ideal angular momentum maximizing the total flux interacting with the device. Such a device also needs to be chiral, so as to preferentially scatter the incident light into angular momentum of a particular handedness.

These basic principles appear to be obeyed by the majority of optically-driven rotating devices developed so far.

2.2. Analogy with Holograms Interacting with Paraxial Beams

Interestingly, the above principles describing the interaction between the driving beam and target object are essentially the same as the symmetry principles describing the interaction between a hologram (i.e., a thin phase object) and a paraxial Laguerre–Gauss beam.[17]

Indeed, an optically-driven microrotor can be thought of as a microhologram interacting with a focussed beam. Therefore, one should aim for a half-wave phase difference between light that passes through the structure and light that does not. Such a design philosophy can be fruitful, allowing simple design of microrotors and even microscopic optical elements to introduce orbital angular momentum into a driving beam.[3]

3. QUANTITATIVE MODELLING

While the principles outlined above allow choice of size and rotational symmetry of a optically-rotated microobject, and an estimate of optimum thickness based on the microhologram concept, quantitative modelling can prove highly valuable for exploring the effects of variation in shape, material and driving beam. This has much in common with the problem of modelling typical optical tweezers; the key difference is that the particle is no longer spherical. Methods for the modelling of optical trapping of simple nonspherical objects provides a suitable starting point. An ideal method is the T-matrix method, essentially the extension of Lorenz–Mie theory to nonspherical particles.[18] In particular, this allows rapid repeated calculations as the illumination of an object is varied, providing, for example, a means by which the optimum incident driving beam can be found.

However, the usual methods for calculating the T-matrix of a nonspherical particle[12,19] generally fail for particle geometries far from spherical. On the other hand, the T-matrix method is more properly a *description* of the scattering properties of an object, and, in principle, a wide variety of methods can be used to calculate it.

Considering the structure of typical optical micromachines, we believe that an ideal method is the discrete dipole approximation (DDA), also known as the coupled dipole method.[20,21] In DDA, the scattering object is represented as a collection of dipole scatterers, and the total scattering problem, including the coupling between the dipoles, is solved. DDA is well-suited to modelling optical micromachines. Firstly, only the volume of the actual particle needs to be discretized, while both the particle and surrounding medium in a volume enclosing the particle are discretized in other general methods such as the finite-difference time-domain method (FDTD) and finite element methods (FEM). Considering that structures as shown in figure 1 are not unusual, where the particle occupies only a relatively small fraction of the nearby volume, this can mean a considerable saving in required memory and time. Secondly, DDA performs well for relatively low contrast scatterers, which is typical of most optical micromachines so far, usually constructed of a polymer material and deployed in a dielectric liquid. Thirdly, it is relatively simple to obtain the T-matrix via DDA if repeated calculations are desired.[22] Finally, it is possible to exploit discrete rotational symmetry of a particle to reduce the computational resources, including both time and memory, by orders of magnitude. This last factor is important, since optical micromachines are often large in overall dimension compared to the wavelength (while having wavelength scale features forcing the use of electromagnetic theory rather than geometric optics), and the available resources can place such devices beyond practical calculation.[23] Figure 1 shows a typical case.

We will proceed to describe the modelling of optical micromachines using DDA, with emphasis on the use of symmetry to optimize the calculations.

3.1. DDA Theory

The scatterer is represented by point dipoles (figure 1(b) labelled by an index $j = 1, ..., N$, each with polarizability tensor α_j, and located at position $\vec{r}_j$. In the presence of a field, each dipole will have a dipole moment of $\vec{P}_j = \alpha_j \vec{E}_j$, where α_j is the polarizability tensor and $\vec{E}_j$ is the time-harmonic electric field amplitude at $\vec{r}_j$. This field will be equal to the sum of the incident field and the contributions from the other $N - 1$ dipoles,

$$\vec{E}_j = \vec{E}_{inc,j} - \sum_{k \neq j} \bar{A}_{jk} \vec{P}_k, \tag{4}$$

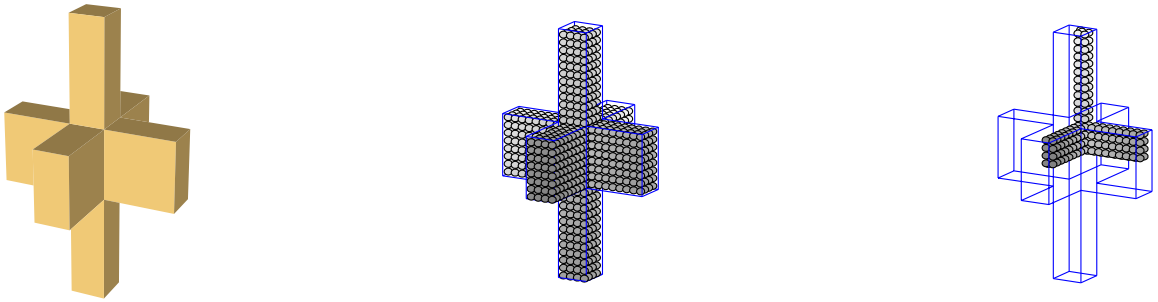

(a) (b) (c)

Figure 1. (a) An optically-driven microrotor. (b) Discrete dipole representation of the rotor. (c) Discrete rotational and mirror symmetries allow the modelling of only the repeated segment, with a major reduction in required memory and time.

where the interaction matrix $\bar{A}_{jk}$ is given by

$$\bar{A}_{jk} = \frac{\exp(\mathrm{i}kr_{jk})}{r_{jk}} \left[k^2(\hat{r}_{jk}\hat{r}_{jk} - I_3) + \frac{\mathrm{i}kr_{jk} - 1}{r_{jk}^2}(3\hat{r}_{jk}\hat{r}_{jk} - I_3) \right], \; j \neq k, \tag{5}$$

where r_{jk} is the distance from $\vec{r}_j$ to $\vec{r}_k$, and $\hat{r}_{jk}$ is the unit vector directed from $\vec{r}_j$ to $\vec{r}_k$. Defining $\bar{A}_{jj} = \alpha_j^{-1}$, the problem is reduced to solving for the unknown dipole moments $\vec{P}_k$ in the following system of $3N$ linear equations:

$$\sum_{k=1}^{N} \bar{A}_{jk}\vec{P}_k = \vec{E}_{inc,j}. \tag{6}$$

Once $\vec{P}_j$ is known, the field, force and torque can be calculated.

3.2. Exploiting Rotational Symmetry

The size of the microdevices we intend to model may exceed 10–20 wavelengths in size, which may well require computational time in excess of several days and RAM beyond that available. To circumvent these limitations, we exploit the rotational and/or mirror symmetry of a microcomponent. This is closely tied with the link between DDA and the T-matrix method. In the T-matrix method, the fields are represented as sums of vector spherical wavefunctions (VSWFs),[12,19] and to use DDA to calculate a T-matrix, we can simply calculate the scattered field (and its VSWF representation) for each possible incident single-mode VSWF field in turn. The important point is that each VSWF is characterized by a simple azimuthal dependence of $\exp(\mathrm{i}m\phi)$, where m is the azimuthal mode index.

If we consider a group of dipoles that are rotationally symmetric about the vertical axis—in the case of figure 2(a), there is 4th-order rotational symmetry—the magnitude of the incident field will be the same, the field differing only by a phase dependent on the azimuthal $\exp(\mathrm{i}m\phi)$ factor. Only the dipole moment of one repeating unit of the total number of dipoles needs to be known.

This brings up question of how to reduce the number of equations such that only one rotational unit needs to be solved. Conventionally, the interaction matrix as defined in (5) represents the coupling between each dipole with all other dipoles. Figure 3(a) shows the interaction matrix for the example set of dipoles shown in figure 2(b). In general the matrix will be made up of $N \times N$ cells for N dipoles; each cell is a 3×3 tensor. In the example, the matrix is made up of 8×8 cells. A diagonal cell represents the self interaction (or the inverse of the polarizability) and an off-diagonal cell represents the coupling between different dipoles. Taking advantage of the equal amplitudes and known phase factors between a dipole and its rotational counterparts, we can reduce the interaction matrix. Taking the example in figure 2(c), we contruct the interaction matrix as if there were

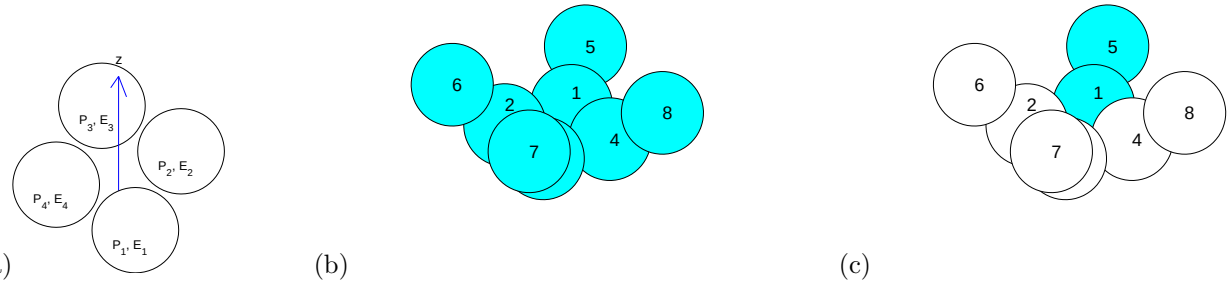

(a) (b) (c)

Figure 2. (a) Rotationally symmetric arrangement of dipoles. (b) 8-dipole example. (c) The 2 dipoles required to completely specify all dipole moments.

only 2 dipoles but we aggregate the contribution from the appropriate dipoles. For the off-diagonal cells, the coupling between a dipole with the other dipoles including their rotational counterparts are summed as follows

$$\bar{A}_{jk} = \sum_{m=1}^{M} \frac{\exp(\mathrm{i}kr_{jk}(m))}{r_{jk}(m)} \left[k^2(\hat{r}_{jk}(m)\hat{r}_{jk}(m) - I_3) + \frac{\mathrm{i}kr_{jk}(m) - 1}{r_{jk}^2(m)}(3\hat{r}_{jk}(m)\hat{r}_{jk}(m) - I_3) \right], \; j \neq k, \tag{7}$$

where M is the order of discrete rotational symmetry, $r_{jk}(m)$ is the distance from points r_j to the rotationally symmetric points $r_k(m)$, and $\hat{r}_{jk}(m)$ is the vector from points r_j to $r_k(m)$. For the diagonal cells, the "self interaction" includes the coupling between a dipole and its rotational counterparts:

$$\bar{A}_{jj} = \alpha_j^{-1} + \sum_{m=2}^{M} \frac{\exp(\mathrm{i}kr_{jk}(m))}{r_{jk}(m)} \left[k^2(\hat{r}_{jk}(m)\hat{r}_{jk}(m) - I_3) + \frac{\mathrm{i}kr_{jk}(m) - 1}{r_{jk}^2(m)}(3\hat{r}_{jk}(m)\hat{r}_{jk}(m) - I_3) \right], \; j = k. \tag{8}$$

Figure 3(b) shows the interaction matrix representation for the example dipole system in figure 2(c). The compressed interaction matrix is a factor of M^2 smaller than the conventional matrix.

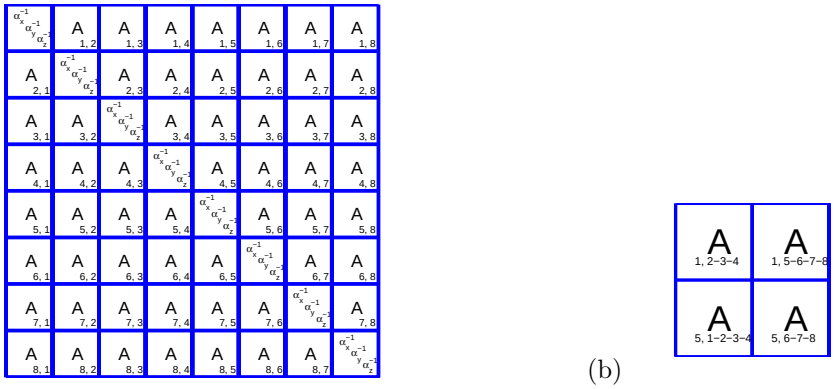

(a) (b)

Figure 3. (a) Full interaction matrix. (b) Symmetry reduced interaction matrix

Having precalculated the incident fields $\vec{E}_{j,inc}$ at each dipole of the rotational unit, we solve for the polarizations $\vec{P}_j$ for the dipoles with a reduced set of linear equations. The polarizations of the rotational counterpart dipoles can be calculated by applying the known phase factor.

We can exploit mirror symmetry in a similar fashion, since the VSWFs possess either even or odd parity w.r.t. the xy-plane. This allows a reduction in size by a further factor of 4.

4. FABRICATION OF OPTICAL MICROMACHINES

Photopolymerization is a promising technology for the rapid optical fabrication of microstructures and microdevices. The method was first reported in 1993, with structures including a microvalve, a coil spring 50 μm in

diameter with a height of 250 μm, and a pipe with an inner diameter of 30 μm.[24] These were fabricated using a xenon lamp as a UV source, focused into a liquid resin. The resin hardened only in the focal spot of the UV beam and by scanning the sample over the focus 3D objects could be obtained.

The resolution of such optically fabricated microstructures is determined by the size of the smallest solidified volume, or "voxel" (volumetric pixel). For the above-mentioned objects, the resolution was $5 \times 5 \times 3\mu\text{m}^3$. The resolution can be substantially increased if, instead of using one-photon absorption of UV light, one uses two-photon absorption of IR light. The increase in resolution is due to the fact that two-photon absorption probability is proportional to the square of light intensity and hence the resin polymerizes in a far smaller volume than in one-photon absorption. The two-photon polymerization technique was pioneered by Strickler and Webb in 1991 ,[25] following the application of two-photon excitation in two-photon laser scanning fluorescence microscopy.[26] The first 3D structures microfabricated using two-photon polymerization were reported in 1997.[27] They were spiral structures with a diameter of 6 μm and a wire width of 1.3 μm. Since then, various micromachines have been produced (micropumps, microgears, microneedles) with high resolution.[28–30] A lot of research is being done in order to improve the spatial resolution of the photopolymerization process and objects with fabrication accuracy of 150 nm have been reported.[31]

4.1. Method

We use the NOA series of UV curing resins from Norland Products to produce and investigate microstructures. They are based on a mixture of photoinitiator molecules and thiol-ene monomers. These resins are photopolymerized when exposed to light in the UV range with $\lambda < 400$ nm and require an energy flux of 2–4.5 J/cm^2 for a full cure. The two-photon polymerization is performed in an in-house-built inverted microscope. A scheme of the setup is shown in figure 4.

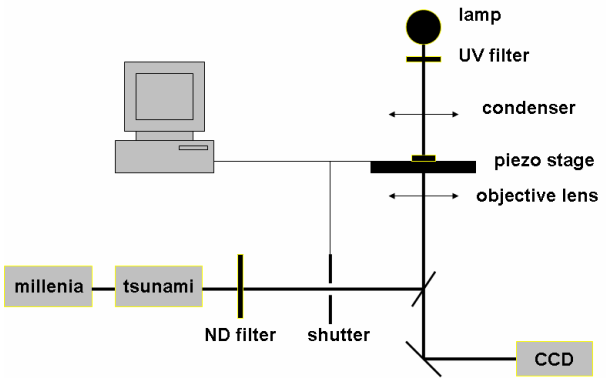

Figure 4. Experimental setup for microfabrication.

For two-photon polymerization we use infrared light ($\lambda = 780$ nm) produced by a femtosecond pulse Ti:Sapphire laser (Tsunami, Spectra Physics) pumped by a 532 nm solid state laser (Millenia, Spectra Physics). The pulse length is 80 fs with an 80 MHz repetition rate. The laser beam is attenuated to the power needed for polymerization and then passes through a computer controlled shutter and is reflected into the objective lens by a dichroic mirror. The objective lens is an Olympus 100× oil immersion lens with high numerical aperture NA = 1.3 to achieve high spatial resolution. The sample is mounted on a computer controlled piezo stage (model P-611.3S, PI, Physik Instrumente) and is imaged onto a CCD with the same objective lens. The travel range of the piezo stage is 100 μm in x, y and z directions. The resin sample is sandwiched between two glass coverslips which are separated by an adhesive spacer with a thickness of 120 μm. 3D structures are fabricated by raster scanning the resin sample over the laser beam using the piezo stage. A scheme of the fabrication method is shown in figure 5.

The 3D object is represented by a sequence of 2D layers (stored as bitmap files) corresponding to the areas that need to be scanned. The program controlling the scanning stage reads the bitmap files and the resin is exposed (the shutter is opened) when the pixel in the bitmap is black (has value 0). 3D structures are obtained by moving the sample in the z direction after each xy scan. The bitmap resolution is set to 100×100 pixels

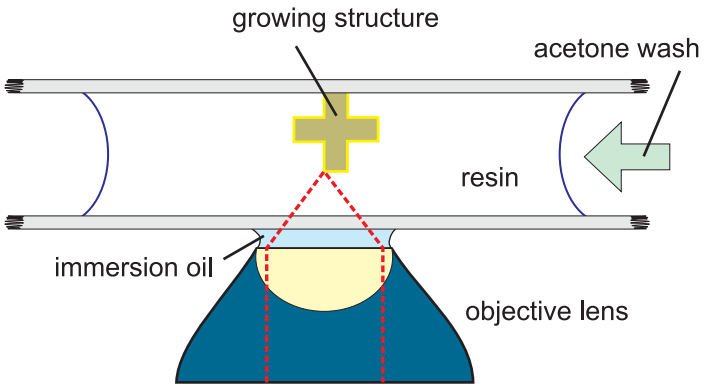

Figure 5. Schematics of the microfabrication method.

which corresponds to 10 μm $\times$10 μm travel in the x and y directions; hence, each individual pixel is 100×100 nm. The steps in the z direction are 200 nm. The structures are grown upside down on the upper coverslip. This top-down scanning method has the advantage that the laser beam does not pass through already exposed resin on the way to the focus, reducing the possibility of distortion of the focal spot.

After the polymerization, the unexposed resin is washed off with acetone, leaving the 3D structure attached to the coverslip. The 3D structures are characterized with a scanning electron microscope (SEM) and bright-field optical microscopy. The first structures we produced were 3D chiral objects with 4-fold rotational symmetry (off-set crosses) which are ideal as optically driven microrotors[1,7] (figure 6). Optical microscope images of the produced structures in unpolymerized resin and after rinsing with acetone are shown in figures 7(a) and 7(b) respectively. A typical SEM image is shown in figure 8. The layer-by-layer formation of the microstructure can be clearly seen in the SEM image. Due to the high travel range of the scanning stage, one could produce a large number of microstructures at once, which is a big advantage in terms of fabrication efficiency. The fabrication time for each structure is about 15 minutes.

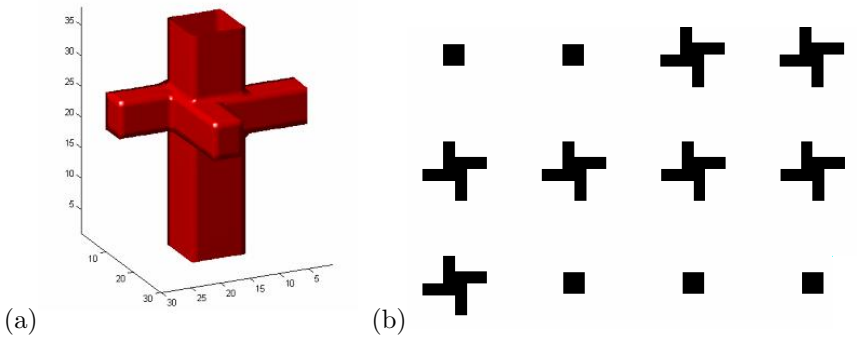

Figure 6. (a) Design of off-set cross optical microrotor. (b) Bitmap sequence describing the rotor.

The off-set cross rotors were then optically trapped and rotated. The trap was a typical optical tweezers trap using a 1064 nm Nd:YAG fiber laser. The off-set crosses could be three-dimensionally trapped, and would rotate in linearly polarized light. With a laser power of 100 mW (before the objective), the rotation frequency was about 2 Hz.

5. CONCLUSIONS

The coupling of qualitative design principles with quantitative modelling and rapid microfabrication and testing of prototype devices provides a powerful and versatile process for the design, engineering, and testing of optically-

(a) 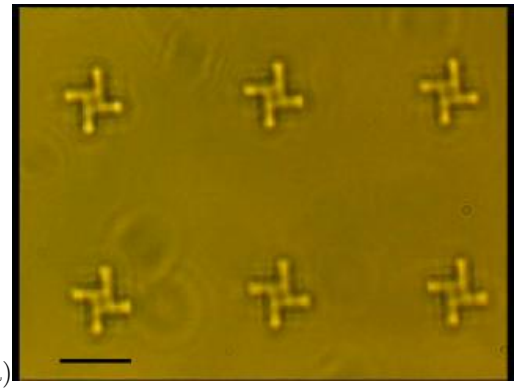 (b) 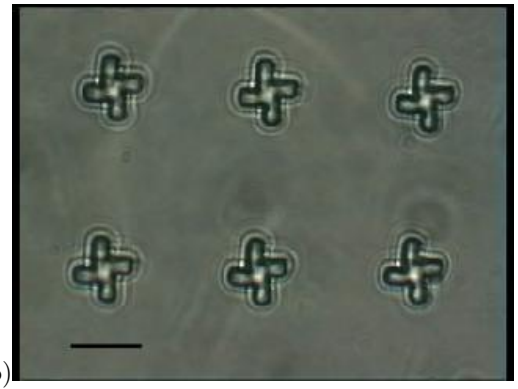

Figure 7. Optical microscope images of the 3D off-set crosses produced by two-photon polymerization. (a) In unpolymerized resin. (b) After rinsing. Scale bars are 5 μm.

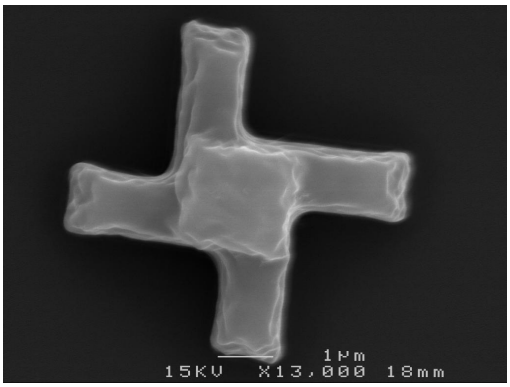

Figure 8. SEM image of the 3D off-set cross.

driven micromachines.

We have outlined a set of qualitative principles that can be used for developing an initial design, and have described an algorithm ideally suited for the quantitative calculation of optical forces and torques on such structures. Finally, we have described our method for rapid prototyping and report the successful testing of a structure based on our general design principles.

REFERENCES

1. T. A. Nieminen, J. Higuet, G. Knöner, V. L. Y. Loke, S. Parkin, W. Singer, N. R. Heckenberg, and H. Rubinsztein-Dunlop, "Optically driven micromachines: progress and prospects," *Proc. SPIE* **6038**, pp. 237–245, 2006.
2. L. Kelemen, S. Valkai, and P. Ormos, "Integrated optical motor," *Applied Optics* **45**, pp. 2777–2780, 2006.
3. G. Knöner, S. Parkin, T. A. Nieminen, V. L. Y. Loke, N. R. Heckenberg, and H. Rubinsztein-Dunlop, "Integrated optomechanical microelements," *Optics Express* **15**, pp. 5521–5530, 2007.
4. N. A. Umov, *Izbrannye Sochineniya (Selected Works)*, Gostexizdat, Moscow, 1950. (In Russian).
5. T. A. Nieminen, G. Knöner, N. R. Heckenberg, and H. Rubinsztein-Dunlop, "Physics of optical tweezers," in *Laser Manipulation of Cells and Tissues*, M. W. Berns and K. O. Greulich, eds., *Methods in Cell Biology* **82**, ch. 6, pp. 207–236, Elsevier, Amsterdam, 2007.
6. J. Courtial and M. J. Padgett, "Limit to the orbital angular momentum per unit energy in a light beam that can be focussed onto a small particle," *Optics Communications* **173**, pp. 269–274, 2000.
7. T. A. Nieminen, S. J. Parkin, N. R. Heckenberg, and H. Rubinsztein-Dunlop, "Optical torque and symmetry," *Proc. SPIE* **5514**, pp. 254–263, 2004.

8. A. E. Siegman, *Lasers*, Oxford University Press, Oxford, 1986.
9. M. Padgett and L. Allen, "Light with a twist in its tail," *Contemporary Physics* **41**, pp. 275–285, 2000.
10. M. Padgett, J. Courtial, and L. Allen, "Light's orbital angular momentum," *Physics Today* **57**, pp. 35–40, May 2004.
11. J. E. Curtis and D. G. Grier, "Structure of optical vortices," *Physical Review Letters* **90**, 133901, 2003.
12. P. C. Waterman, "Symmetry, unitarity, and geometry in electromagnetic scattering," *Physical Review D* **3**, pp. 825–839, 1971.
13. T. A. Nieminen, "Comment on "Geometric absorption of electromagnetic angular momentum", C. Konz, G. Benford," *Optics Communications* **235**, pp. 227–229, 2004.
14. M. E. J. Friese, T. A. Nieminen, N. R. Heckenberg, and H. Rubinsztein-Dunlop, "Optical alignment and spinning of laser trapped microscopic particles," *Nature* **394**, pp. 348–350, 1998. Erratum in *Nature* **395**, p. 621, 1998.
15. A. I. Bishop, T. A. Nieminen, N. R. Heckenberg, and H. Rubinsztein-Dunlop, "Optical application and measurement of torque on microparticles of isotropic nonabsorbing material," *Physical Review A* **68**, 033802, 2003.
16. M. Born and E. Wolf, *Principles of Optics*, Cambridge University Press, Cambridge, 6th ed., 1997.
17. S. J. Parkin, T. A. Nieminen, N. R. Heckenberg, and H. Rubinsztein-Dunlop, "Optical measurement of torque exerted on an elongated object by a noncircular laser beam," *Physical Review A* **70**, 023816, 2004.
18. T. A. Nieminen, N. R. Heckenberg, and H. Rubinsztein-Dunlop, "Computational modelling of optical tweezers," *Proc. SPIE* **5514**, pp. 514–523, 2004.
19. T. A. Nieminen, H. Rubinsztein-Dunlop, and N. R. Heckenberg, "Calculation of the T-matrix: general considerations and application of the point-matching method," *Journal of Quantitative Spectroscopy and Radiative Transfer* **79-80**, pp. 1019–1029, 2003.
20. E. M. Purcell and C. R. Pennypacker, "Scattering and absorption of light by nonspherical dielectric grains," *Astrophysical Journal* **186**, pp. 705–714, 1973.
21. B. T. Draine and P. J. Flatau, "Discrete-dipole approximation for scattering calculations," *Journal of the Optical Society of America A* **11**, pp. 1491–1499, Apr. 1994.
22. D. W. Mackowski, "Discrete dipole moment method for calculation of the t matrix for nonspherical particles," *Journal of the Optical Society of America A* **19**, pp. 881–893, 2002.
23. W. L. Collett, C. A. Ventrice, and S. M. Mahajan, "Electromagnetic wave technique to determine radiation torque on micromachines driven by light," *Applied Physics Letters* **82**, pp. 2730–2732, 2003.
24. K. Ikuta and K. Hirowatari, "Real three dimensional micro fabrication using stereo lithography and metal moulding," *Proceedings of the IEEE Workshop on MEMS* , pp. 42–47, 1993.
25. J. H. Strickler and W. W. Webb, "Three-dimensional optical data storage in refractive media by two-photon point excitation," *Optics Letters* **16**, pp. 1780–1782, 1991.
26. W. Denk, J. H. Strickler, and W. W. Webb, "Two-photon laser scanning fluorescence microscopy," *Science* **248**, pp. 73–76, 1990.
27. S. Maruo, O. Nakamura, and S. Kawata, "Three-dimensional microfabrication with two-photon-absorbed photopolymerization," *Optics Letters* **22**, pp. 132–134, 1997.
28. S. Maruo and H. Inoue, "Optically driven micropump produced by three-dimensional two-photon microfabrication," *Applied Physics Letters* **89**, 144101, 2006.
29. S. Maruo, K. Ikuta, and H. Korogi, "Submicron manipulation tools driven by light in a liquid," *Applied Physics Letters* **82**, pp. 133–135, 2003.
30. P. Galajda and P. Ormos, "Complex micromachines produced and driven by light," *Applied Physics Letters* **78**, pp. 249–251, 2001.
31. S. Kawata, H.-B. Sun, T. Tanaka, and K. Takada, "Finer features for functional microdevices," *Nature* **412**, pp. 697–698, 2001.